# Structural Elucidation of Fullerene Dimers by High-Resolution Ion Mobility Measurements and Trajectory Calculation Simulations

**Alexandre A. Shvartsburg, Robert R. Hudgins, Philippe Dugourd,† and Martin F. Jarrold***

*Department of Chemistry, Northwestern University, 2145 Sheridan Road, Evanston, Illinois 60208*

*Received: November 13, 1996; In Final Form: January 2, 1997*[⊗]

$C_{120}$, $C_{130}$, and $C_{140}$ cluster anions and cations produced by laser desorption of fullerene films have been examined by high-resolution ion mobility measurements and trajectory calculation simulations. The results for anions and cations are similar. Two peaks are present in the measured drift time distributions. They are attributed to fullerene cage isomers and dimers. The fullerene peak is broad, indicating the presence of a range of fullerene cages with different shapes. The measured mobilities of the dimers are in good agreement with mobilities determined by trajectory calculations for the [2 + 2] cycloadduct geometries of $(C_{60})_2$, $C_{60}$·$C_{70}$, and $(C_{70})_2$. Comparison of the mobilities calculated for the dimer geometries by the commonly used hard-sphere projection approximation with those determined by trajectory calculations with a realistic potential shows that the projection approximation significantly underestimates the inverse mobilities. The deviations, which are large enough to assign the observed features to the wrong geometries, result mainly from the complete neglect of the scattering process in the hard-sphere projection approximation.

## Introduction

Fullerenes oligomerize with relative ease to produce metastable dimers and polymers, in both the solid state[1] and the gas phase.[2] The structure of the solid state $(C_{60})_n$ oligomers has been the object of intense theoretical and experimental research. The $C_{60}$ polymer prepared by Rao et al.[1] by UV irradiation of fullerene samples has been identified as a [2 + 2] cycloadduct.[3−6] The same bonding has been proposed for a number of $C_{60}$ polymer phases synthesized under a variety of conditions.[7−10] Similar processes also occur for alkali metal fullerides. The orthorhombic chains in $RbC_{60}$ and $KC_{60}$ apparently polymerize via the same [2 + 2] cycloaddition process.[11−17] Recently, a distinct, "dimer" phase of these fullerides has been produced at low temperature.[17−23] This phase is thought to consist of $C_{60}$ dimers covalently bound by single C-C bonds.[17,19−23] Polymerization of bulk $C_{70}$ has also been achieved by UV irradiation,[5,24,25] but with much lower efficiency than with $C_{60}$ under the same conditions, and the polymer structure has not yet been elucidated.

Free fullerene dimers have also been extensively studied, but almost exclusively by theoretical means as model systems for the elementary units of $C_{60}$ and $C_{70}$ polymers.[17,24−34] The existence of $C_{60}$ and $C_{70}$ dimers in the gas phase has been reported,[25,35] but the only previous experimental investigation of their structure was by Hunter et al.[2] They used ion mobility measurements[36] to examine the $C_{120}^+$ ions generated by laser desorption of fullerene films and found two poorly resolved peaks which they attributed to a closed cage fullerene and a dimer. However, it was not possible to distinguish between several plausible dimer geometries at that time. Hunter et al.[2] also examined the annealing and dissociation pathways for the dimer and estimated their activation energies.

We have now revisited this problem taking advantage of the dramatic enhancement in both our experimental capabilities and the methods used to calculate mobilities. The mobilities for $C_{120}^{+/-}$, $C_{130}^{+/-}$, and $C_{140}^{+/-}$ have been measured on our new high-resolution ion mobility apparatus,[37] which provides more than an order of magnitude improvement in resolving power compared with that available from the injected ion drift tube apparatus used in the previous experiments.[2] Structural information is deduced from ion mobility measurements by calculating mobilities for trial geometries and comparing them to the measured values. We have recently developed the computational tools to calculate mobilities of polyatomic ions by trajectory calculations using a realistic intermolecular potential.[38] The mobilities calculated by this method for all the dimer geometries considered here are significantly different from those obtained using the widely used hard-sphere projection approximation. The deviations are large enough that the wrong structural assignments would be made if this model is employed. It appears that the main problem with the projection approximation here is that it completely neglects the scattering process between the ion and the buffer gas.[39]

## Experimental Methods

The high-resolution ion mobility apparatus employed in these studies has been described in detail elsewhere.[37] Briefly, the apparatus consists of a source region which is directly coupled to a 63 cm long drift tube. Both of them contain helium buffer gas at a pressure of 500−520 Torr. The ions are generated by pulsed 308 nm laser desorption of an unpurified fullerene film deposited on a copper rod. After formation, the ions are directed by shaped electric fields to a small aperture in the ion gate that separates the source region from the drift tube. The function of the ion gate is to prevent neutral species from entering the drift tube from the source region. The ion gate consists of a 0.5 cm diameter by 2.5 cm long channel with a uniform electric field along its length. A flow of helium buffer gas through the ion gate, from the drift tube into the source region, prevents neutral species from entering the drift tube, while the electric field pulls the ions against the flow. The ions then travel along the length of the drift tube under the influence of a uniform electric field generated by a stack of isolated rings and a voltage divider. At the end of the drift tube, some of the ions exit through a small aperture. They are then focused into a quadrupole mass spectrometer, and at the end of the quadrupole

† Permanent and present address: Laboratoire de Spectrometrie Ionique et Moleculaire (UMR No. 5579), CNRS et Université Lyon I, bat. 205, 43 Bd. du 11 Novembre 1918, 69622 Villeurbanne Cedex, France.

⊗ Abstract published in *Advance ACS Abstracts,* February 1, 1997.

S1089-5639(96)03790-5 CCC: $14.00 

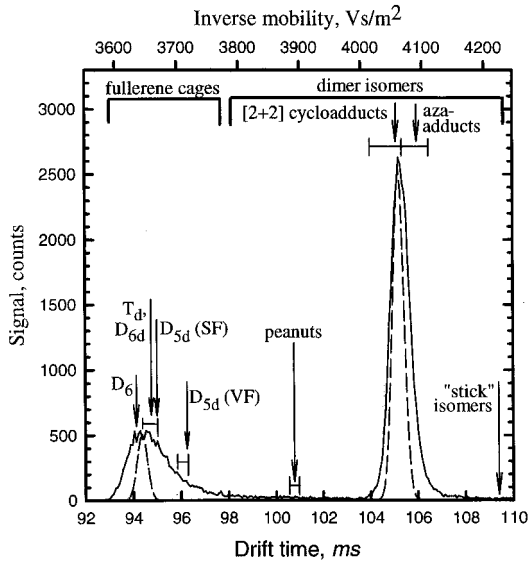


**Figure 1.** Drift time distribution measured for $C_{120}^-$ from laser desorption of a fullerene film. The drift times determined for various candidate geometries by trajectory calculations are superimposed. The horizontal bars show the range of values obtained for the geometries discussed in the text; the arrows show the highest level result for a particular structure of the neutral. The dashed line shows the drift time distributions expected for a single isomer assuming that all the ions are produced at the same point on the target rod.

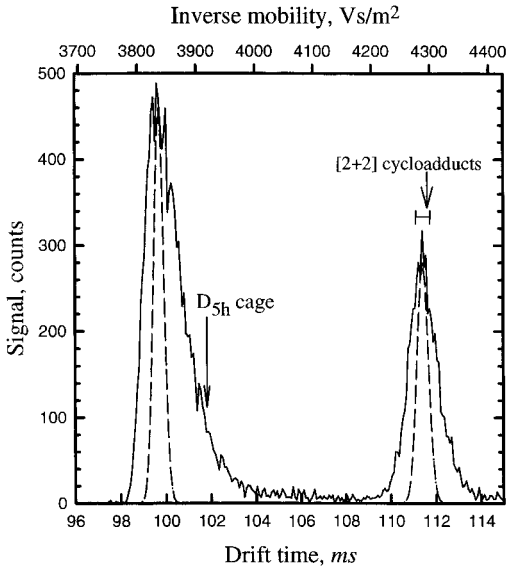


**Figure 2.** Drift time distribution measured for $C_{130}^-$ from laser desorption of a fullerene film. The drift times determined for the $D_{5h}$ fullerene cage and [2 + 2] cycloadduct by trajectory calculations are indicated by the arrows. The horizontal bar shows the uncertainty in the calculated mobility of [2 + 2] cycloadduct as explained in the text. The dashed line shows the drift time distributions expected for a single isomer assuming that all the ions are produced at the same point on the target rod.

they are detected by an off-axis collision dynode and dual microchannel plates. Drift time distributions are recorded with a multichannel scaler using the laser pulse as the start trigger. All measurements were performed with the drift tube at 25 °C.

## Results

Figure 1 shows part of a drift time distribution measured for $C_{120}^-$ from desorption of a fullerene film at a low laser power. There is no signal outside of the range of drift times shown in the figure (92−110 ms). It is customary to express ion mobility data in terms of inverse reduced mobilities, which are proportional to the orientationally averaged collision integrals.[40] A scale showing these inverse mobilities is given on the top of Figure 1. Two clearly resolved peaks are present in the distribution. Drift time distributions recorded for $C_{120}$ cations were similar to those recorded for the anions. The relative abundances of the two peaks are sensitive to the laser pulse energy employed; at higher desorption laser fluences the relative abundance of the dimer decreases. The distribution presented here is similar to those presented previously[2] for $C_{120}^+$, except for the order of magnitude improvement in the resolution. In the previous measurements, the two peaks shown in Figure 1 were only partially resolved. The two isomers separated for $C_{120}^{+/-}$ are due to a closed cage fullerene, at shorter drift times, and a dimer. We have also measured the mobility of $C_{120}$ anions generated by laser vaporization of a graphite rod (Ultra Carbon, Ultra F). Only one peak is observed, it is narrower and shifted to slightly (∼1%) shorter times than the fullerene cage isomer produced from the fullerene film. The dashed lines in Figure 1 show the drift time distributions calculated for a single isomer,[40] assuming that the ions are generated at the same point on the target rod. For the dimer isomer, the measured peak is slightly broader than the peak calculated for a single isomer. Some of this difference results from the finite size of the laser beam on the target rod. For the closed cage fullerene the measured peak is substantially broader than that expected for a single isomer, indicating the presence of several fullerene cage isomers with different shapes. At higher laser powers the fullerene peak becomes narrower and shifts toward the position of the $C_{120}$ peak from graphite, while the dimer peak broadens.

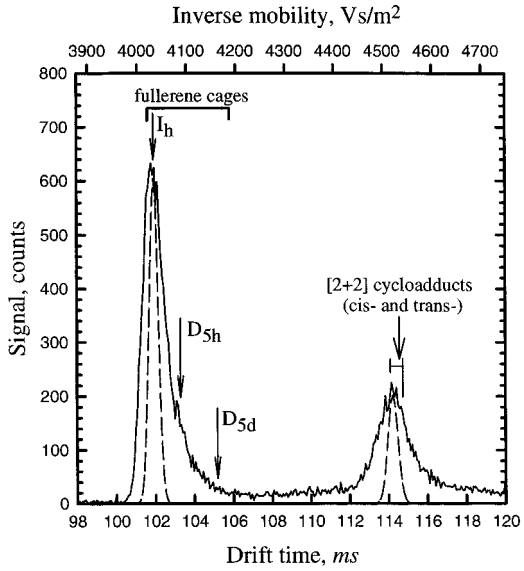


**Figure 3.** Drift time distribution measured for $C_{140}^-$ from laser desorption of a fullerene film. The drift times determined for various candidate geometries by trajectory calculations are superimposed (indicated by arrows). The horizontal bar shows the uncertainty in the calculated mobility of [2 + 2] cycloadduct as explained in the text. The dashed line shows the drift time distributions expected for a single isomer assuming that all the ions are produced at the same point on the target rod.

We have also studied the $C_{130}$ and $C_{140}$ ions which are produced in significant abundance by laser desorption of an unpurified fullerene film due to the presence of $C_{70}$. The drift time distributions measured for $C_{130}^-$ and $C_{140}^-$ at intermediate and high laser powers, respectively, are shown in Figures 2 and 3, respectively. The overall picture for these clusters closely resembles that for $C_{120}^{+/-}$: there is a broad fullerene peak at a drift time slightly longer than that of the fullerene cage produced

by laser vaporization of graphite and a narrower (at low laser power) dimer peak. Drift time distributions recorded for the anions and cations are similar. The abundance of the dimer decreases with increasing laser power, while the fullerene peak narrows and the dimer peak broadens. The fullerene peaks show a tail that extends to longer drift times.

### Mobility Calculations

Structural information is extracted from ion mobility measurements by calculating mobilities for candidate geometries and comparing them to the experimental values. In the low field limit, where the mobility is independent of drift field, the mobility is given by[40]

$$K = \frac{(18\pi)^{1/2}}{16}\left[\frac{1}{m}+\frac{1}{m_B}\right]\frac{ze}{(k_BT)^{1/2}}\frac{1}{\Omega_{avg}^{(1,1)}}\frac{1}{N} \qquad (1)$$

where $m$ and $m_B$ are respectively the masses of the ion and of the buffer gas atom, $N$ is the buffer gas number density, $ze$ is the ionic charge, $T$ is the gas temperature, and $\Omega_{avg}^{(1,1)}$ is the orientationally averaged collision integral or collision cross section. We have determined $\Omega_{avg}^{(1,1)}$ using trajectory calculations[38] with a realistic potential. This treatment requires a major effort and commitment of computer resources. So to see whether this expense is really warranted, we have also calculated mobilities with the widely used hard-sphere projection approximation[41−43] and by an exact hard-spheres scattering model.[39] The collision integral should be evaluated by averaging the momentum transfer cross section over the relative velocity between the buffer gas atom and the ion. And the momentum transfer cross section should be determined by averaging a function of the scattering angle over the impact parameter and collision geometry. The scattering angle is the angle between the incoming and outgoing trajectories in a collision between the buffer gas atom and the ion. The procedure described above is implemented in our classical trajectory calculations.[38] The projection approximation and the exact hard-spheres scattering model treat the evaluation of the collision integral less rigorously. The simple projection approximation[41−43] totally ignores all the details of the scattering process between the ion and the buffer gas by replacing the average collision integral in eq 1 with the average geometric cross section. The exact hard-spheres scattering model[39] treats the scattering process properly in the limit of hard-sphere interatomic potentials. Both of these models obviously ignore the long-range interactions between the ion and buffer gas atom. Calculations using the projection approximation and the exact hard-spheres scattering model require hard-sphere collision distances between C and He. These were obtained by fitting the measured mobility of $C_{60}^{+/-}$ at 25 °C.[39] For the trajectory calculations we have employed a pairwise additive Lennard-Jones potential plus a charge-induced dipole component with the charge delocalized over all of the atoms.[38] The Lennard-Jones parameters for this potential ($\sigma = 3.043$ Å and $\epsilon = 1.34$ meV, where $\epsilon$ is the depth and $\sigma$ is the distance where the potential becomes positive) were obtained by fitting the measured mobilities of $C_{60}^{+}$ fullerene over an 80−400 K temperature range.[38,44] The mobilities obtained from these three different models differ significantly. In the following we will employ values derived from the most reliable method, trajectory calculations with a realistic potential. The differences are discussed further below.

For $C_{120}$ fullerene, five different cage isomers have been optimized by Scuseria and collaborators[45,46] and Adams et al.:[47] an almost spherical $D_6$ geometry, a pearl-shaped $T_d$, a tubular $D_{6d}$, and two elongated $D_{5d}$ structures, side-facing (SF) and vertex-facing (VF). The calculated inverse mobilities for these clusters are plotted in Figure 1. The values for $D_{6d}$ and $T_d$ geometries are identical within statistical error, while those for $D_6$ and $D_{5d}$ SF are only marginally smaller and greater, respectively. These cages could not be separated even with the greatly improved resolving power available here. The broad flat top of the fullerene peak may be due to the presence of all these isomers in comparable abundances. The mobility of $D_{5d}$ VF cage differs from those of the other four by >1%, and it should be clearly resolved. There is some signal in the position allocated for this isomer. It is therefore possible that the $D_{5d}$ VF isomer is a minor component. Theory indicates that this is a relatively high-energy isomer.[26,45−47] In any case, our data prove the existence of several $C_{120}$ fullerene cages with different gross shapes, including the elongated isomers. Hundreds of $C_{120}$ cages satisfy the isolated pentagon rule.[45]

Numerous families of isomers have been considered in the literature for the $C_{60}$ dimer. A partial list, in order of increasing center-to-center distance, is (a) multiply bonded hexagon−hexagon and pentagon−pentagon facing adducts (8.3−8.5 Å),[29] (b) fused fullerenes[26] (peanuts) (8.4−8.6 Å), (c) direct [2 + 4] cycloadducts[26] (8.6 Å), (d) [2 + 2] cycloadducts[26−33] (9.1 Å), (e) singly-bonded (aza) isomers[17,33] (9.3−9.4 Å), (f) stick-bridged isomers[26] (10.4 Å), and (g) [2 + 2] handles cycloadducts[26] (10.6 Å). The center-to-center distances are the tight-binding values (a) and MNDO values for neutral clusters scaled by 0.9884 (all other cases). Scaling by this factor brings the MNDO coordinates for $C_{60}$ into agreement[38] with the X-ray and electron diffraction data,[48] and all MNDO coordinates employed here were scaled in this way. Coordinates obtained by other theoretical methods were not scaled, unless noted. No geometries have been published for singly charged $C_{60}$ dimers. So we have computed inverse mobilities for singly charged dimers using the coordinates for the neutral and dianion dimer geometries determined by semiempirical MNDO (b, d−f),[17,26,33] AM1 and PM3 (d, e),[33] the tight-binding models of Pederson and co-workers (d)[30,31] and Sankey and co-workers (a, d),[29] and Hartree−Fock and B3LYP (d, e).[17] The calculated inverse mobilities for dimers (b, d−f) are superimposed on the measured drift time distribution in Figure 1. In some cases a range of values is shown, as the calculated inverse mobility depends slightly on the theoretical method employed to optimize geometry and on the charge state. The mobility of fullerene dimers is set largely by the center-to-center distance of the two cages, and the measured mobility is consistent with a distance of about 9.2 Å. This excludes all of the possible families listed above except for (d) the [2 + 2] cycloadducts and (e) the aza adducts. There are four [2 + 2] isomers and two aza adducts that differ in the orientation of cages with respect to connecting bond(s). The calculated inverse mobilities for these adducts depend slightly on the method of geometry optimization, the charge state, and the particular isomer. The calculated values lie in the range 4010−4070 V s/m$^2$ for the [2 + 2] adducts and 4060−4115 V s/m$^2$ for the aza adducts. The measured value for the dimer isomer is 4070 ± 10 V s/m$^2$.

The capsular $D_{5h}$ isomer is the only optimized cage geometry available for $C_{130}$.[47] Its calculated inverse mobility is significantly larger than that of the $C_{130}$ fullerene peak (see Figure 2), though it still lies within the broad tail extending to longer drift times. For $C_{140}$, three cage isomers have been optimized:[47] near-spherical $I_h$ and elongated $D_{5h}$ and $D_{5d}$. The measured mobility of $C_{140}$ fullerene is in perfect agreement with the value calculated for $I_h$ isomer (4030 V s/m$^2$), whereas the values expected for the $D_{5h}$ and $D_{5d}$ cages, which are calculated[47] to be less stable

than the $I_h$ isomer, correspond to the broad tail of our experimental peak. We are not aware of any investigations of $C_{60}$·$C_{70}$ adducts. Theory suggests[24,25] that two $C_{70}$ cages can make a [2 + 2] cycloadduct; however, only the five bonds joining pentagons in each polar cap are reactive. This would restrict the addition of $C_{60}$ to $C_{70}$ to one of 10 identical sites on $C_{70}$. We obtained a structure for the $C_{60}$·$C_{70}$ cluster by joining halves of the $(C_{60})_2$ [2 + 2] and $(C_{70})_2$ [2 + 2] cycloadducts optimized by Menon et al.[25,27] The coordinates of these dimers were scaled so that the coordinates for $(C_{60})_2$ more closely matched those obtained from AM1, PM3, B3LYP, and scaled MNDO. The calculated inverse mobility for the constructed $C_{60}$·$C_{70}$ geometry is in the range 4280−4300 V s/m$^2$ (depending on the scaling) while the value measured for $C_{60}$·$C_{70}$ is 4295 ± 10 V s/m$^2$. For the $C_{70}$ dimer, the same regioselectivity could result in cis and trans isomers with respect to the connecting four-membered ring. The calculated inverse mobility for the trans isomer[25] (4515−4540 V s/m$^2$ depending on the scaling) matches our measured value (4525 ± 10 V s/m$^2$) exactly. The cis isomer has not been considered in the literature. A structure for this isomer was generated from *trans*-$(C_{70})_2$ by cutting this dimer in half and rotating about the connecting bonds. The resulting *cis*-$(C_{70})_2$ has the same mobility, within the statistical error of our calculation, as the trans isomer, and so the dimer peak of $C_{140}$ could correspond to either or both of these species.

## Discussion

The $C_{120}^{+/-}$ fullerene cages derived from the fullerene films have broader peaks in the drift time distributions than the cages produced by laser vaporization of graphite, particularly at low desorption laser powers. The $C_{120}^{+/-}$ cages produced from fullerene films clearly result from the coalescence of two $C_{60}$ fullerenes. Several groups have studied this coalescence process.[49,50] Conversion of a dimer geometry into a single fullerene cage involves substantial rearrangement, which should start with the formation of a "peanut" structure,[26] and then proceed through a variety of capsular or elongated cage isomers. All theoretical studies indicate that elongated fullerene cages are less stable than the more spherical ones.[26,45−47] Therefore, it seems likely that the broad distribution of fullerene isomers observed at low laser fluences results from the quenching of metastable, elongated fullerene geometries before they have converted into the most stable fullerene isomer. As noted above, the fullerene peak narrows and shifts to slightly shorter times as the laser fluence is increased. This is consistent with the extra heat generated by the increased laser power, annealing more of the elongated cages into lower energy near-spherical cages. The fullerene cage peaks for $C_{130}^{+/-}$ and $C_{140}^{+/-}$ are also broader when these clusters are derived from the fullerene film, presumably for the reasons discussed above.

The ion mobility measurements for the $C_{60}$ dimer are consistent with either a [2 + 2] cycloadduct or a singly-bonded (aza) geometry. The [2 + 2] geometry is the most plausible, for the following reasons. Hunter et al.[2] have estimated that the activation energy for dissociation of $(C_{60})_2^+$ is 1.5 eV. This is similar to the value of 1.25 eV found by Eklund and co-workers[4] for the activation energy for the dissociation of the bulk [2 + 2] $C_{60}$ polymer. The latest calculations[31] yield a value of ≤1.6 eV for the dissociation energy of the neutral [2 + 2] dimer. The single bond in the aza adduct is reported to be much weaker,[21,23] and the aza adduct only appears to form in the solid state when the [2 + 2] pathway is inhibited by the steric hindrance that occurs in solid fullerides below the transition temperature for free rotation.[19−21,51,52] All the theoretical methods that have been applied (semiempirical,[17,26,28,33] various tight binding schemes,[26,27] density functional based methods,[17,28,29] and Hartree−Fock[17]) predict the [2 + 2] cycloadduct to be the lowest energy structure for neutral $(C_{60})_2$ and the lowest or second lowest for $(C_{60})_2^{2-}$. For $C_{60}$·$C_{70}$ and $(C_{70})_2$ the measured mobilities for the dimer isomers are also consistent with a [2 + 2] geometry formed at a 5−5 bond of $C_{70}$. Theory[24,25] also suggests that this structure is the lowest energy for $(C_{70})_2$.

**TABLE 1: Inverse Mobilities (V s/m$^2$) of Several $(C_{60})_2$ Isomers Evaluated Using the Projection Approximation, the Exact Hard-Spheres Scattering Model (EHSSM), and Trajectory Calculations[a]**

| geometry | projection approxn | EHSSM | trajectory calcn |
|---|---|---|---|
| Peanut[26] 56/56 | 3808 | 3906 | 3882 |
| [2 + 2] 66/66 cycloadduct[26] | 3882 | 4035 | 4047 |
| aza adduct, trans[33] | 3916 | 4076 | 4091 |
| 5−6 stick[26] | 4032 | 4204 | 4222 |

[a] All geometries are optimized for neutrals using MNDO and scaled by 0.9884 as explained in the text.

The inverse mobilities discussed above were obtained by trajectory calculations using a realistic potential. This treatment is quite computationally intensive so it is instructive to compare the results of these calculations with those obtained from the simple hard-sphere projection approximation that has been widely used to calculate mobilities. The comparison is shown in Table 1, where calculated inverse mobilities are shown for a variety of $C_{60}$ dimer geometries. It appears that the projection approximation underestimates the inverse mobilities of the dimers by over 4%. This is significant because agreement between measured and calculated mobilities of better than 2% has been introduced[43,53] as a criterion for assigning geometries to carbon clusters using mobility measurements. The fact that both models were calibrated using the measured mobility of $C_{60}^{+/-}$ makes the poor agreement particularly disconcerting. The measured inverse mobility for the $C_{60}$ dimer is 4070 ± 10 V s/m$^2$. With the projection approximation, the only isomer that has a calculated inverse mobility close to the measured value is a stick-bridged geometry (0.9% difference). Therefore, the projection approximation would have led us to make the wrong structural assignments. As discussed above, the projection approximation ignores long-range interactions between ions and buffer gas atoms and replaces the collision integral by the average geometric cross section so that it does not treat the scattering properly. In particular, it ignores multiple scattering.[39] Inverse mobilities calculated for $(C_{60})_2$ by the exact hard-spheres scattering model[39] are also shown in Table 1. The exact hard-spheres scattering model also ignores the long-range interactions but treats the scattering process rigorously for a hard-sphere potential. The mobilities given by this model for all geometries of $(C_{60})_2$, $C_{60}$ $C_{70}$, and $(C_{70})_2$ considered here are within 0.6% of those determined from trajectory calculations. This indicates that the main deficiency in the projection approximation in this case is its failure to treat the scattering process properly. This is not surprising because the C−He potential that we used was normalized for $C_{60}^{+/-}$, and the difference between the effective potential of a fullerene and a fullerene dimer is small. However, regardless of the origin of the discrepancy, it is obvious that the simple projection approximation is inadequate and that it is desirable to perform mobility calculations with a more rigorous model to avoid assigning the observed features to the wrong geometries.

**Acknowledgment.** We gratefully acknowledge the National Science Foundation (CHE-9306900) and Petroleum Research

Fund administered by the American Chemical Society for support of this work. P. Dugourd also acknowledges the financial support from the CNRS and NATO. We thank Dr. G. B. Adams, Prof. J. Kurti, Dr. M. Menon, Dr. M. Pederson, Prof. O. F. Sankey, Prof. G. E. Scuseria, Dr. D. L. Strout, and Prof. K. Subbaswamy for kindly providing us their calculated coordinates of various fullerene cage and dimer isomers. We are also grateful to J. L. Fye for his help with the experimental work and to Prof. G. C. Schatz for numerous helpful discussions.

## References and Notes

(1) Rao, A. M.; Zhou, P.; Wang, K. A.; Hager, G. T.; Holden, J. M.; Wang, Y.; Lee, W. T.; Bi, X. X.; Eklund, P. C.; Cornett, D. S.; Duncan, M. A.; Amster, I. J. *Science* **1993**, *259*, 955.

(2) Hunter, J. M.; Fye, J. L.; Boivin, N. M.; Jarrold, M. F. *J. Phys. Chem.* **1994**, *98*, 7440.

(3) Zhou, P.; Dong, Z. H.; Rao, A. M.; Eklund, P. C. *Chem. Phys. Lett*. **1993**, *211*, 337.

(4) Wang, Y.; Holden, J. M.; Bi, X. X.; Eklund, P. C. *Chem. Phys. Lett*. **1994**, *217*, 413.

(5) Eklund, P. C.; Rao, A. M.; Zhou, P.; Wang, Y.; Holden, J. M. *Thin Solid Films* **1995**, *257*, 185.

(6) Tanaka, K.; Matsuura, Y.; Oshima, Y.; Yamabe, T.; Asai, Y.; Tokumoto, M. *Solid State Commun*. **1995**, *93*, 163. Goze, C.; Rachdi, F.; Hajji, L.; Nunez-Regueiro, M.; Marques, L.; Hodeau, J. L.; Mehring, M. *Phys. Rev. B* **1996**, *54*, R3676.

(7) Oszlanyi, G.; Forro, L. *Solid State Commun*. **1995**, *93*, 265.

(8) Xu, C. H, Scuseria, G. E. *Phys. Rev. Lett.* **1995**, *74*, 274.

(9) Iwasa, Y.; Arima, T.; Fleming, R. M.; Siegrist, T.; Zhou, O.; Haddon, R. C.; Rothberg, L. J.; Lyons, K. B.; Carter, H. L.; Hebard, A. F.; Tycko, R.; Dabbagh, G.; Krajewski, J. J.; Thomas, G. A.; Yagi, T. *Science* **1994**, *264*, 1570. Nunez-Regueiro, M.; Marques, L.; Hodeau, J. L.; Bethoux, O.; Perroux, M. *Phys. Rev. Lett*. **1995**, *74*, 278.

(10) Takahashi, N.; Dock, H.; Matsuzawa, N.; Ata, M. *J. Appl. Phys*. **1993**, *74*, 5790.

(11) Chauvet, O.; Oszlanyi, G.; Forro, L.; Stephens, P. W.; Tegze, M.; Faigel, G.; Janossy, A. *Phys. Rev. Lett.* **1994**, *72*, 2721.

(12) Stephens, P. W.; Bortel, G.; Faigel, G.; Tegze, M.; Janossy, A.; Pekker, S.; Oszlanyi, G.; Forro, L. *Nature* **1994**, *370*, 636.

(13) Pekker, S.; Forro, L.; Mihaly, L.; Janossy, A. *Solid State Commun*. **1994**, *90*, 349.

(14) Pekker, S.; Janossy, A.; Mihaly, L.; Chauvet, O.; Carrard, M.; Forro, L. *Science* **1994**, *265*, 1077.

(15) Stafstrom, S.; Boman, M.; Fagerstrom, J. *Europhys. Lett*. **1995**, *30*, 295.

(16) Harigaya, K. *Phys. Rev. B* **1995**, *52*, 7968.

(17) Scuseria, G. E. *Chem. Phys. Lett.* **1996**, *257*, 583.

(18) Martin, M. C.; Koller, D.; Rosenberg, A.; Kendziora, C.; Mihaly, L. *Phys. Rev. B* **1995**, *51*, 3210.

(19) Zhu, Q.; Cox, D. E.; Fischer, J. E. *Phys. Rev. B* **1995**, *51*, 3966.

(20) Oszlanyi, G.; Bortel, G.; Faigel, G.; Tegze, M.; Granasy, L.; Pekker, S.; Stephens, P. W.; Bendele, G.; Dinnebier, R.; Mihaly, G.; Janossy, A.; Chauvet, O.; Forro, L. *Phys. Rev. B* **1995**, *51*, 12228.

(21) Pusztai, T.; Faigel, G.; Granasy, L.; Tegze, M.; Pekker, S. *Europhys. Lett*. **1995**, *32*, 721.

(22) Petit, P.; Robert, J.; Fischer, J. E. *Phys. Rev. B* **1995**, *51*, 11924.

(23) Granasy, L.; Kemeny, T.; Oszlanyi, G.; Bortel, G.; Faigel, G.; Tegze, M.; Pekker, S.; Forro, L.; Janossy, A. *Solid State Commun*. **1996**, *97*, 573. Oszlanyi, G.; Bortel, G.; Faigel, G.; Granasy, L.; Bendele, G. M.; Stephens, P. W.; Forro, L. *Phys. Rev. B* **1996**, *54*, 11849.

(24) Rao, A. M.; Menon, M.; Wang, K. A.; Eklund, P. C.; Subbaswamy, K. R.; Cornett, D. S.; Duncan, M. A.; Amster, I. J. *Chem. Phys. Lett.* **1994**, *224*, 106.

(25) Menon, M.; Rao, A. M.; Subbaswamy, K. R.; Eklund, P. C. *Phys. Rev. B* **1995**, *51*, 800.

(26) Strout, D. L.; Murry, R. L.; Xu, C.; Eckhoff, W. C.; Odom, G. K.; Scuseria, G. E. *Chem. Phys. Lett*. **1993**, *214*, 576.

(27) Menon, M.; Subbaswamy, K. R.; Sawtarie, M. *Phys. Rev. B* **1993**, *49*, 13966.

(28) Matsuzawa, N.; Ata, M.; Dixon, D. A.; Fitzgerald, G. *J. Phys. Chem.* **1994**, *98*, 2555.

(29) Adams, G. B.; Page, J. B.; Sankey, O. F.; O'Keeffe, M. *Phys. Rev. B* **1994**, *50*, 17471.

(30) Pederson, M. R.; Quong, A. A. *Phys. Rev. Lett*. **1995**, *74*, 2319.

(31) Porezag, D.; Pederson, M. R.; Frauenheim, T.; Kohler, T. *Phys. Rev. B* **1995**, *52*, 14963.

(32) Fagerstrom, J.; Stafstrom, S. *Phys. Rev. B* **1996**, *53*, 13150.

(33) Kurti, J.; Nemeth, K. *Chem. Phys. Lett*. **1996**, *256*, 119.

(34) Surjan, P. R.; Udvardi, L.; Nemeth, K. *Synth. Met.* **1996**, *77*, 107.

(35) Cornett, D. S.; Amster, I. J.; Duncan, M. A.; Rao, A. M.; Eklund, P. C. *J. Phys. Chem*. **1993**, *97*, 5036.

(36) Hagen, D. F. Anal. Chem. **1979**, *51*, 871. St. Louis, R. H.; Hill, H. H. *Crit. Rev. Anal. Chem*. **1990**, *21*, 321. von Helden, G.; Hsu, M. T.; Kemper, P. R.; Bowers, M. T. *J. Chem. Phys*. **1991**, *95*, 3835.

(37) Dugourd, Ph.; Hudgins, R. R.; Clemmer, D. E.; Jarrold, M. F. *Rev. Sci. Instrum*., in press.

(38) Mesleh, M. F.; Hunter, J. M.; Shvartsburg, A. A.; Schatz, G. C.; Jarrold, M. F. *J. Phys. Chem*. **1996**, *100*, 16082.

(39) Shvartsburg, A. A.; Jarrold, M. F. *Chem. Phys. Lett.* **1996**, *261*, 86.

(40) Mason, E. A.; McDaniel, E. W. *Transport Properties of Ions in Gases*; Wiley: New York, 1988.

(41) Mack Jr., E. *J. Am. Chem. Soc*. **1925**, *47*, 2468.

(42) Lin, S. N.; Griffin, G. W.; Horning, E. C.; Wentworth, W. E. *J. Chem. Phys*. **1974**, *60*, 4994.

(43) von Helden, G.; Hsu, M. T.; Gotts, N. G.; Bowers, M. T. *J. Phys. Chem*. **1993**, *97*, 8182.

(44) The values for the Lennard-Jones parameters employed here ($\sigma =$ 3.043 Å and $\epsilon = 1.34$ meV) are slightly different from those given in ref 38 ($\sigma = 3.068$ Å and $\epsilon = 1.34$ meV). Both sets of values fit the measured mobilities for $C_{60}^+$ over an 80−400 K temperature range equally well.

(45) Scuseria, G. E. In *Buckminsterfullerenes*; Billups, W. E., Ciufolini, M. A., Eds.; VCH Publishers: Weinheim, 1993; p 103.

(46) Murry, R. L.; Colt, J. R.; Scuseria, G. E. *J. Phys. Chem*. **1993**, *97*, 4954.

(47) Adams, G. B.; Sankey, O. F.; Page, J. B.; O'Keeffe, M.; Drabold, D. A. *Science* **1992**, *256*, 1792.

(48) Liu, S.; Lu, Y.-J.; Kappes, M. M.; Ibers, J. A. *Science* **1991**, *254*, 408. Hedburg, K.; Hedburg, L.; Bethune, D. S.; Brown, C. A.; Dorn, H. C.; Johnson, R. D.; de Vries, M. *Science* **1991**, *254*, 410.

(49) Yeretzian, C.; Hansen, K.; Diederich, F.; Whetten, R. L. *Nature* **1992**, *359*, 44. Yeretzian, C.; Hansen, K.; Diederich, F.; Whetten, R. L. *Z. Phys. D* **1993**, *26*, S300. Hansen, K.; Yeretzian, C.; Whetten, R. L. *Chem. Phys. Lett*. **1994**, *218*, 462.

(50) Beck, R. D.; Weis, P.; Brauchle, G.; Kappes, M. M. *J. Chem. Phys*. **1994**, *100*, 262.

(51) Winter, J.; Kuzmany, H. *Phys. Rev. B* **1995**, *52*, 7115.

(52) Kamaras, K.; Granasy, L.; Tanner, D. B.; Forro, L. *Phys. Rev. B* **1995**, *52*, 11488.

(53) Lee, S.; Gotts, N. G.; von Helden, G.; Bowers, M. T. *Science* **1995**, *267*, 999.